Journal of Electroanalytical Chemistry 738 (2015) 40–46

Contents lists available at ScienceDirect

Journal of Electroanalytical Chemistry

journal homepage: www.elsevier.com/locate/jelechem

Studies of the electrochemical behavior of moniliformin mycotoxin and its sensitive determination at pretreated glassy carbon electrodes in a non-aqueous medium

Paulo César Díaz Toro, Fernando Javier Arévalo, María Alicia Zon *, Héctor Fernández *

Grupo de Electroanalítica (GEANA), Departamento de Química, Facultad de Ciencias Exactas, Físico-Químicas y Naturales, Universidad Nacional de Río Cuarto, Agencia Postal N° 3, 5800 Río Cuarto, Argentina

ARTICLE INFO

Article history:
Received 17 September 2014
Received in revised form 12 November 2014
Accepted 17 November 2014
Available online 25 November 2014

Keywords:
Moniliformin
Electrochemical oxidation
Cyclic voltammetry
Square wave voltammetry
Thermodynamic and kinetics parameters

ABSTRACT

The electrochemical oxidation of moniliformin (MON) mycotoxin in acetonitrile (ACN) + 0.1 mol dm^{-3} $(C_4H_9)_4NPF_6$ at electrochemically pretreated glassy carbon electrodes (EPGCE) and fiber disk carbon ultramicroelectrodes (FCUME) is studied for the first time. Electrochemical techniques used were cyclic (CV), convolution and square wave (SWV) voltammetries as well as controlled potential electrolysis. Experimental results allowed inferring a complex electro-oxidation mechanism with adsorption of reactant and homogeneous chemical steps coupled to the electron transfer reaction.

The UV–Vis spectroscopy was used as a non-electrochemical technique in order to follow the disappearance/appearance of the reactant/reaction product/s during controlled potential electrolysis.

The most probable electro-oxidation mechanism proposed on the base of digital simulation results of cyclic voltammograms is one of the CEC type. Thermodynamic and kinetics parameters were calculated from the fitting of experimental cyclic voltammograms, while the diffusion parameter was calculated from convoluted cyclic voltammograms. We propose that reaction products obtained are produced through the decomposition of the MON radical generated from the electrochemical oxidation of MON anion.

On the other hand, the MON quantitative determination was performed using adsorptive SWV at EPGCE. An extremely low detection limit of 1×10^{-11} mol dm^{-3} (1.2 ppt) for a signal to noise ratio of 3:1 was calculated.

1. Introduction

Moniliformin (MON), whose IUPAC name is 3-hydroxy-3-cyclobutene-1,2-dione, is a mycotoxin produced by a large number of species of *Fusarium*, mainly *F. proliferatum* [1]. Cole et al. [2] were the first to isolate MON from infected United States maize. Springer et al. [3] were who first elucidated the MON chemical structure. MON is usually present as its sodium (NaMON) or potassium (KMON) salts (Fig. 1). It is water soluble, given that the free acid has a very low pK_a [4].

The mechanism of toxicity of MON is not yet well known, and its toxic-kinetics is still unknown [5]. It has been proposed that MON inhibits the oxidation of intermediates in the tricarboxylic acid cycle [6–8], causing respiratory diseases, and myocardial degeneration in animals, and leading in some cases to death. It is also proposed that MON competes with pyruvate for the active sites of the enzymes α-ketoglutarate dehydrogenase, pyruvate decarboxylase, and aceto-hydroxy acid synthetase [9].

It has not yet been found evidence of the carcinogenic or mutagenic activity of MON in humans. However, an endemic disease produced in China, called Keshan disease, was related to MON, considering that the symptoms produced in humans were similar to those previously observed in studies of animals intoxicated with MON [10]. The oral toxicity of MON in rats has been studied by a liquid-chromatography-mass spectroscopy method [5].

However, MON is considered an emerging mycotoxin, international laws have not yet established maximum permitted levels in grains and food [1,10,11]. Consequently, developing sensitive analytical methods for MON is highly needed. Several techniques have been proposed for assay of MON. Chromatographic techniques are usually the most used to detect and quantify mycotoxins [1,12]. The use of strong anion exchange columns for cleanup prior to HPLC coupled to high-resolution mass spectrometry analysis was described to be a suitable alternative technique for the

* Corresponding authors. Tel.: +54 358 4676440.
E-mail addresses: azon@exa.unrc.edu.ar, alicia_zon@hotmail.com (M.A. Zon), hfernandez@exa.unrc.edu.ar, hfernandezster@gmail.com (H. Fernández).

http://dx.doi.org/10.1016/j.jelechem.2014.11.026
1572-6657/

detection of MON [11,13]. Analytical methods based on immunochemical technology are currently being investigated, but the low molecular weight of MON presents a challenge for this area of research and development [14]. Therefore, the standard methodology to quantify MON requires specific instrumentation and trained operators [14]. As far as we know; there is no report in the literature related to the study of electrochemical properties of MON, and its determination using an electroanalytical method.

In this work, MON electrochemical oxidation is systematically studied for the first time at electrochemically pretreated glassy carbon electrodes (EPGCE) and fiber disk carbon ultramicroelectrodes (FCUME) in acetonitrile (ACN) + 0.1 mol dm^{-3} $(H_9C_4)_4NPF_6$. Compared to untreated glassy carbon electrode (GCE), the EPGCE showed an enhanced signal towards MON oxidation and more reproducible results. Cyclic (CV), convolution, and square wave (SWV) voltammetries, and controlled potential bulk electrolysis were used as the electrochemical techniques. A reaction mechanism for MON electrochemical oxidation is proposed. The quantitative determination of MON was also performed by SWV.

2. Experimental

2.1. Reagents

MON as its sodium salt was purchased from SIGMA Chemical Company and used as received. ACN was Sintorgan (HPLC degree). It was dried over 3 Å molecular sieves during 48 h prior to use. $(H_9C_4)_4NPF_6$ (Fluka, electrochemical degree) was dried at 45 °C in a vacuum oven and stored in a desicator. MON stock solutions (4.2×10^{-3} mol dm^{-3}) were prepared in ACN and kept at 4 °C. Working solutions were prepared daily by adding aliquots of the stock solution to ACN + 0.1 mol dm^{-3} $(H_9C_4)_4NF_6P$.

2.2. Apparatus and experimental measurements

A conventional two-compartment/three electrodes glass cell was used to carry out voltammetric measurements. The working electrode was mainly a GCE disk of 3 mm dia. (Bioanalytical System, USA). However, a CFUME of 10 μm dia. (Bioanalytical System, USA) was used for performing CV measurements at high scan rates (v, up to 11 kV s^{-1}). Prior to each measurement, they were polished to a mirror state with wet alumina powder (0.3 and 0.05 μm from Fischer, respectively), sonicated in a double distilled water bath during 2 min and then dried. The electrochemical area of the GCE was 0.089 cm^2. It was determined as previously discussed [15]. The area of the CFUME was 8.0×10^{-7} cm^2. Optimum EPGCE was obtained by successive sweeps in the potential range from 0.3 to 1.5 V at 0.05 V s^{-1} during five cycles in ACN + 0.1 mol dm^{-3} $(H_9C_4)_4NF_6P$. The counter electrode was a platinum foil of large area ($A \approx 2$ cm^2), and the reference was a commercial Ag/AgCl electrode.

Glass bulk electrolysis cell was one of three-compartment type. A glass fiber paper held in place between the two halves, which separates working and counter electrode compartments. The working electrode was a GC cylindrical bar of area 2.9 cm^2, which was continuously rotated at high speed. The counter electrode was a stainless steel foil of area 16 cm^2.

Cyclic voltammetry (CV) at low scan rates (0.010–0.400 V s^{-1}), square wave voltammetry (SWV), and controlled potential bulk electrolysis were performed using a MicroAutoLab PGSTAT 101 potentiostat (Eco-Chemie, Utrecht, The Netherlands). CV measurements at high scan rates were carried out with a PARC 273 potentiostat, a PARC 175 wave generator, and a HP 5560 digital oscilloscope. The characteristic SW parameters were: amplitude (ΔE_{SW}) = 0.050 V, staircase step height (ΔE_s) = 0.010 V and frequency, f = 10 Hz.

Positive-feedback technique was used to compensate the solution resistance, which was about 100 Ω. Fitting experimental cyclic voltammograms was carried out through BAS DigiSim® software. All experiments were carried out at 25.0 ± 0.2 °C.

3. Results and discussion

3.1. Cyclic and convolution voltammetry's

Fig. 2 shows typical cyclic voltammograms recorded for both blank and MON solutions. A single peak showing a controlled adsorption/diffusion process is observed at a potential of about 0.80 V [16] (see below). In addition, the corresponding cathodic peak is not observed when reversing the direction of the potential sweep, which indicates that chemical and/or electrochemical reaction/s is/are coupled to the initial charge transfer [16–18]. Cyclic voltammograms were also performed in the potential range from 0.00 to −2.00 V and 0.00 to 1.70 V (result not shown). No other peak or peak system appears in the complete potential window. Thus, the MON electrochemical oxidation mechanism is complicated by both a weak adsorption of the reactant and the presence of chemical reaction/s coupled to the electron transfer step.

At a low MON concentration ($c^*_{MON} \approx 8.3 \times 10^{-6}$ mol dm^{-3}), a plot of the anodic peak current ($I_{p,a}$) vs. v was linear, with a correlation coefficient, r = 0.9992, indicating that the oxidation process is mainly controlled by adsorption. From the slope of this plot, i.e., slope = $(2.32 \pm 0.03) \times 10^{-6}$ A s V^{-1}, a value of 3.6×10^{-11} mol cm^{-2} was calculated for the MON surface concentration (Γ_{MON}), being this value lower than that expected for a monolayer coverage [18]. At $c^*_{MON} > 8.3 \times 10^{-6}$ mol dm^{-3}, the oxidation peak shows a mixed control: diffusion/adsorption. This behavior could be also inferred when the working electrode, after recording a cyclic voltammogram in the presence of MON, was rinsed with the

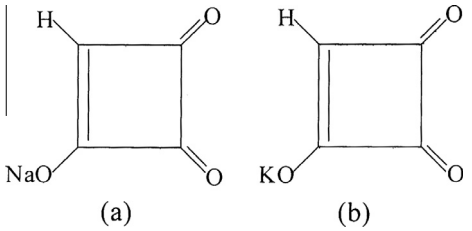

Fig. 1. Chemical structures of sodium (a) and potassium (b) salts of moniliformin.

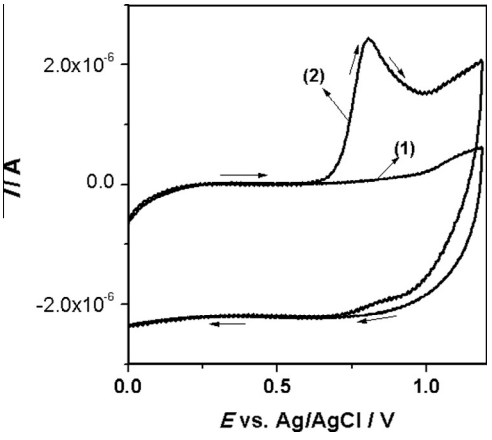

Fig. 2. Cyclic voltammograms of the blank (1) and MON (2) in ACN + 0.1 mol dm^{-3} $(H_9C_4)_4NF_6P$ solution. $c^*_{MON} = 8.3 \times 10^{-5}$ mol dm^{-3}. v = 0.050 V s^{-1}. Working electrode: EPGCE. Arrows indicate the direction of sweep potential.

blank solution and transferred to another electrochemical cell, which contained only the blank solution. Cyclic voltammograms recorded under this experimental condition also showed an irreversible oxidation peak at the same potential range that in the presence of MON, but with smaller currents (results no shown). Thus, the $I_{p,a}$ can be assumed as the sum of the current components of surface and diffusion controlled processes [19]. Thus:

$$I_{p,a}A^{-1} = k_1 v + k_2 v^{1/2} \quad (1)$$

Eq. (1) can be re-written as:

$$I_{p,a} v^{-1/2} A^{-1} = k_1 v^{1/2} + k_2 \quad (2)$$

where $k_1 = \frac{n^2F^2}{4RT}\Gamma_{MON}$, and $k_2 = 2.69 \times 10^5 n^{3/2} D_{MON}^{1/2} c^*_{MON}$, being n the exchanged electron number, D_{MON} the MON diffusion coefficient, A the electrode area and other terms have their usual meaning. Plots of $I_{p,a}\ v^{-1/2}\ A^{-1}$ vs. $v^{1/2}$ were linear. From the intercept and the slope of those plots D_{MON} and Γ_{MON} were determined, respectively, at different MON concentrations (Table 1), assuming $n = 1$ (see below). At low MON concentrations, Γ_{MON} values correspond to the coverage of a sub-monolayer, while at $c^*_{MON} > 1 \times 10^{-3}$ mol dm^{-3} nearly monolayer coverage was obtained. In addition, a value of $(4.8 \pm 0.3) \times 10^{-6}$ cm^2 s^{-1}was calculated for D_{MON}.

Plots of $E_{p,a}$ vs. log v were linear, with slopes varying from 0.058 to 0.053 V/decade mostly, from the highest to the lowest MON concentration, i.e. 3×10^{-3}–8.3×10^{-6} mol dm^{-3}, respectively (results not shown). On the other hand, plots of $E_{p,a}$ vs. log c^*_{MON} are shown in Fig. 3. Interestingly, they show a nearly linear portion with slope close to cero from the lowest concentration used, i.e. 8.3×10^{-6} - mol dm^{-3}, up to about 1×10^{-4} mol dm^{-3} and then $E_{p,a}$ increases with log c^*_{MON} reaching slopes of the order of 0.050–0.060 V/decade for the higher concentration values. In addition, the experimental current function, ($\Psi_E = I_{p,a}/Av^{1/2}c^*_{MON}$) decreases as the scan rate is increased for all concentrations studied (Fig. 4), mainly for higher concentrations, where it can be assumed that adsorption effects are minimized in comparison to diffusion control. Therefore, Ψ_E vs. $v^{1/2}$ plots shift to higher values as the MON concentration decreased. At the higher concentrations of MON the values for Ψ_E were between 0.45 and 0.55, and for the lower concentrations of MON were greater than 1.0 (Fig. 4), showing how the adsorption process renders higher currents for the overall process under experimental conditions where the adsorption process has a greater weight than the diffusion-controlled process.

Besides, current function values indicate that the number of electrons involved in the electrode process is one [18], in good agreement with the results obtained from controlled potential electrolysis measurements (see below).

In addition, D_{MON} was calculated from convoluted cyclic voltammograms recorded at a $c^*_{MON} = 3.0 \times 10^{-3}$ mol dm^{-3} after subtracting background currents (Fig. 5), where the adsorption effects should be minimal. Convoluted currents (I) do not return to zero when the cyclic scan was completed. This behavior indicates that the product of the initial oxidation step is consumed by a homogeneous following chemical reaction coupled to the initial electron transfer reaction [18], in good agreement with results of cyclic voltammetry. A tentative D_{MON} value was calculated considering the convolution model for a EC reaction mechanism, where E indicates

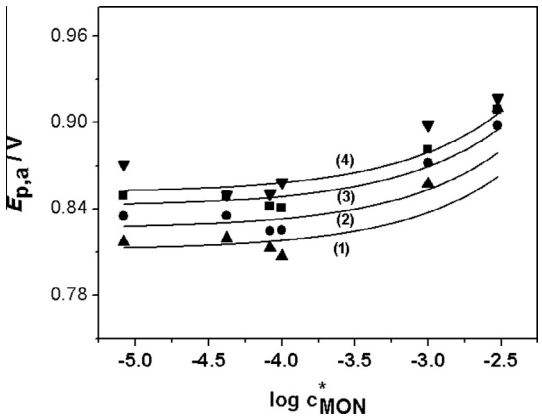

Fig. 3. Dependence of $E_{p,a}$ on log c^*_{MON} at different sweep rates. v: (▲, 1) 0.050; (●, 2) 0.100; (■, 3) 0.200; (▼, 4) 0.300 V s^{-1}. Full symbols: experimental; solid lines: simulated according to Scheme 1. Working electrode: EPGCE.

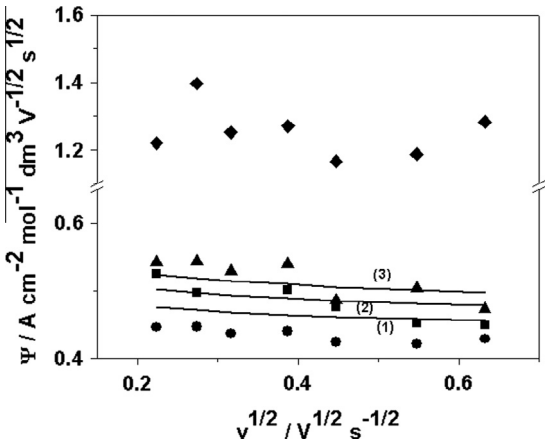

Fig. 4. Dependence of experimental and theoretical current functions (ψ) (see text) on the square root of sweep rate for different MON concentrations. c^*_{MON}: (♦) 4.2×10^{-5}, (▲, 3) 1×10^{-4}, (●, 2) 1×10^{-3} and (■, 1) 3×10^{-3} mol dm^{-3}. Full symbols: experimental; solid lines: simulated according to Scheme 1. Working electrode: EPGCE.

an electron transfer reaction, and C the homogeneous chemical reaction coupled [20], using the following expression:

$$I_L = nFAc^*_{MON}D^{1/2}_{MON} \quad (3)$$

where I_L is the convoluted limiting current. A value of 4.4×10^{-6} - cm^2 s^{-1} was obtained for D_{MON}, which is very close to that calculated from $I_{p,a}\ v^{-1/2}\ A^{-1}$ vs. $v^{1/2}$ plots (see above). A plot of E vs. log $[I_L - I/I]$ was linear in the scan rate range from 0.025 to 0.100 V s^{-1}, with an average slope of – (0.063 ± 0.003) V/decade (r = 0.9921). As expected, this value is close to the theoretical value expected for an uncomplicated EC reaction mechanism, i.e., –0.059/n V at 25 °C (n = 1) for the electrochemical step in the absence of reactant adsorption [20].

On the other hand, cyclic voltammograms performed on UME at high scan rates and intermediate concentration values, where dif-

Table 1
Parameters of linear regression of plots $I_{p,a}\ v^{-1/2}\ A^{-1}$ vs. $v^{1/2}$ as well as values of D_{MON} and Γ_{MON} determined at different MON bulk concentrations.

$10^3\ c^*_{MON}$/mol dm^{-3}	10^5 Intercept/AV$^{-1/2}$ s$^{1/2}$ cm^{-2}	-10^5 Slope/AV^{-1} s cm^{-2}	r	$10^6\ D_{MON}$/cm^2 s^{-1}	$10^{10}\ \Gamma_{MON}$/mol cm^{-2}
0.1	5.85 ± 0.05	1.8 ± 0.1	0.9911	5.1	0.2
1	45.2 ± 0.6	5 ± 1	0.9916	2.9	0.5
3	166 ± 3	45 ± 6	0.9913	5.1	4.9

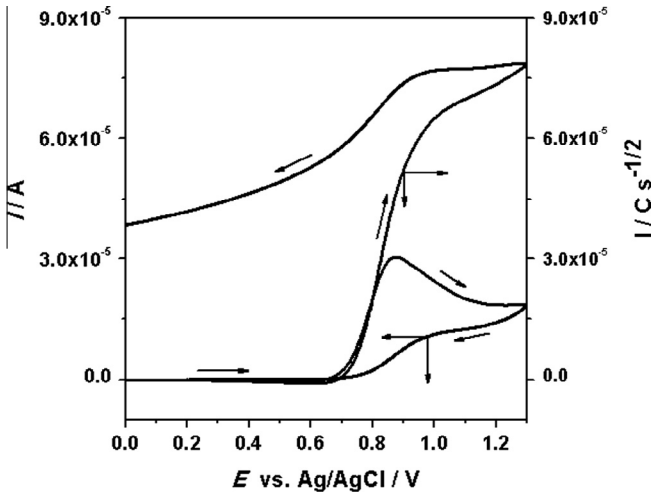

Fig. 5. Cyclic and convoluted cyclic voltammograms of MON in ACN + 0.1 mol dm^{-3} $(H_9C_4)_4NF_6P$, $c^*_{MON} = 3.0 \times 10^{-3}$ mol dm^{-3}, $v = 0.100$ V s^{-1}. Working electrode: EPGCE. Arrows indicate the direction of the potential sweep.

fusion and adsorption phenomena control the electrode process, showed the complementary cathodic peak after the direction of potential sweep was reversed (Fig. 6). Thus, the cathodic peak clearly starts to appears at about $v = 20$–50 V s^{-1} (Fig. 6a), and its peak current increases with v (Fig. 6b). A plot of the difference between the anodic and the cathodic peak potentials, ΔE_p, as a function of v is shown in Fig. 6c. They agree quite well with values calculated from digital simulation (see below). Experimental cathodic to anodic peak current ratios reach a maximum at about 4 kV s^{-1} (Fig. 6d), and then decrease smoothly at higher potential scan rates. $I_{p,c}/I_{p,a}$ values calculated by digital simulation (see below) according to Scheme 1 are shown in Fig. 6d. They also show a maximum in the peak current ratio at about the same rate of potential sweep. Although there are differences between experimental and simulated values of $I_{p,c}/I_{p,a}$ ratios at intermediate values of v, there is a clear trend towards convergence to higher v. We consider that the difference between experimental and simulated values is because the BAS DigiSim® program used to perform the simulation does not allow including adsorption effects of reactant on the whole reaction mechanism. However, the morphology of the experimental $I_{p,c}/I_{p,a}$ vs. v profile coincides reasonably, from a semi-quantitatively point of view, with that predicted by the theory built by Wopschall and Shain [21] for an EC type mechanism with weak reagent adsorption. Therefore, we understand that the results of the peak currents ratios, although semi-quantitative, together with others discussed in this paper are important for the overall interpretation of the data set obtained.

Theoretical cyclic voltammograms at different sweep rates and higher concentrations of the reactant were generated by digital simulation to obtain parameters for diagnostic criteria. They were generated starting from different possible mechanisms involving both heterogeneous and homogeneous reaction steps [18,22–25]. Theoretical current function (Ψ_T) was calculated for different c^*_{MON} and v (in the range of experimental values) from theoretical (simulated) peak currents and compared with the experimental results. We obtained the best fit for a $C_1E_1C_2$ mechanism, as shown in Scheme 1:

where MON^- is the deprotonated MON, $MON^{\cdot}$ is a MON radical and P and Z are the products of the decomposition of the radical. P and Z are not electroactive in the potential range of interest. Theoretical values for $\partial E_{p,a}/\partial \log v$ were in the range from 0.057 to 0.051 V/decade for the MON concentration range of 3.0×10^{-3}–8.3×10^{-6} mol dm^{-3}, in close agreement with the experimental

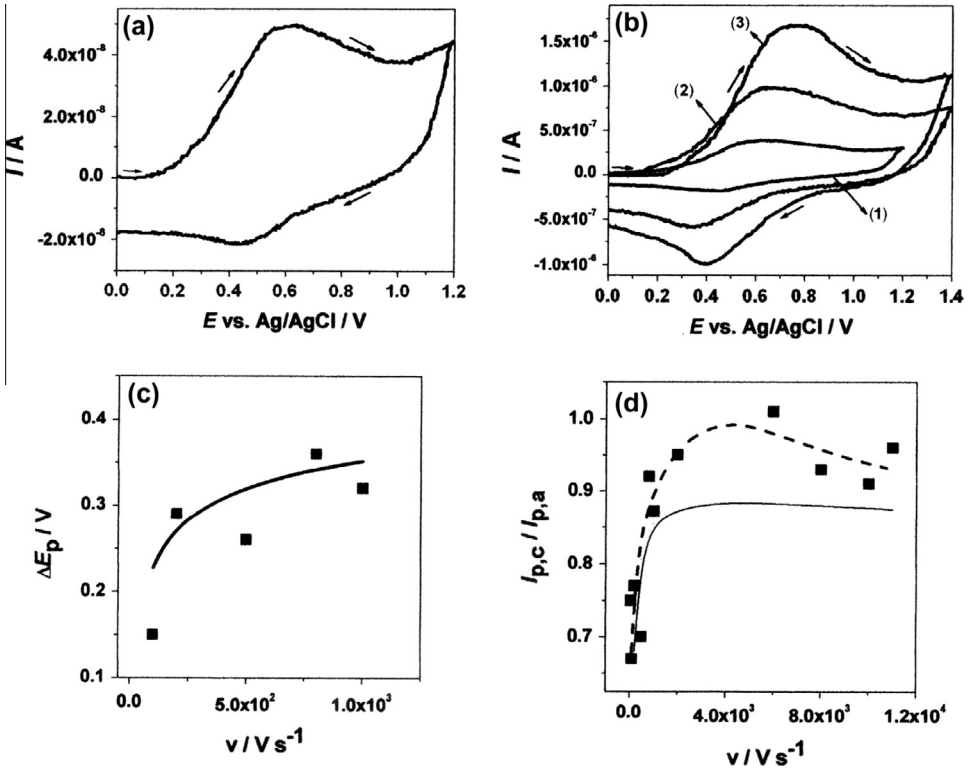

Fig. 6. Cyclic voltammograms recorded for MON in ACN + 0.1 mol dm^{-3} $(H_9C_4)_4NF_6P$ at high scan rates. $c^*_{MON} = 8.3 \times 10^{-5}$ moldm^{-3}. Working electrode: CFUME. Arrows indicate the direction of potential sweep. v = (a) 50 V s^{-1}; (b) 200 (1), 500 (2) and 800 (3) V s^{-1}; (c) plot of ΔE_p vs. $v^{1/2}$; (d) Plot of $I_{p,c}/I_{p,a}$ vs. v. Peak currents were corrected for capacity currents.

$$MON \underset{k_r(1)}{\overset{K(1)}{\rightleftharpoons}} MON^- + H^+ \quad (4)$$

$$MON^- \overset{k_f^0}{\rightleftharpoons} MON^{\cdot} + e^- \quad (5)$$

$$MON^{\cdot} \underset{k_r(2)}{\overset{K(2)}{\rightleftharpoons}} P + Z \quad (6)$$

$$MON \rightleftharpoons P + Z + H^+ + e^- \quad (7)$$

Scheme 1.

values, i.e. 0.058–0.053 V/decade (see above). On the other hand, $E_{p,a}$ vs. $\log c^*_{MON}$ plots follow reasonably well the experimental results (Fig. 4). As it can be observed, the proposed mechanism indicates that the overall reaction involves one electron per one electrolyzed MON molecule, in agreement with experimental results. A reasonably agreement was found between experimental (corrected by blank) and simulated cyclic voltammograms, when the reaction model shown in Scheme 1 was chosen to perform the fitting between experimental and simulated voltammograms (Fig. 7). They strongly agree in their first portion, where the influence of the kinetics of the process is more marked. At potentials more anodic than the peak potential, experimental currents are higher than the simulated ones, which clearly demonstrate the presence of an additional current component due to the oxidation of a certain amount of reactant weakly adsorbed at the electrode surface [21]. On the other hand, it is straightforward to emphasize

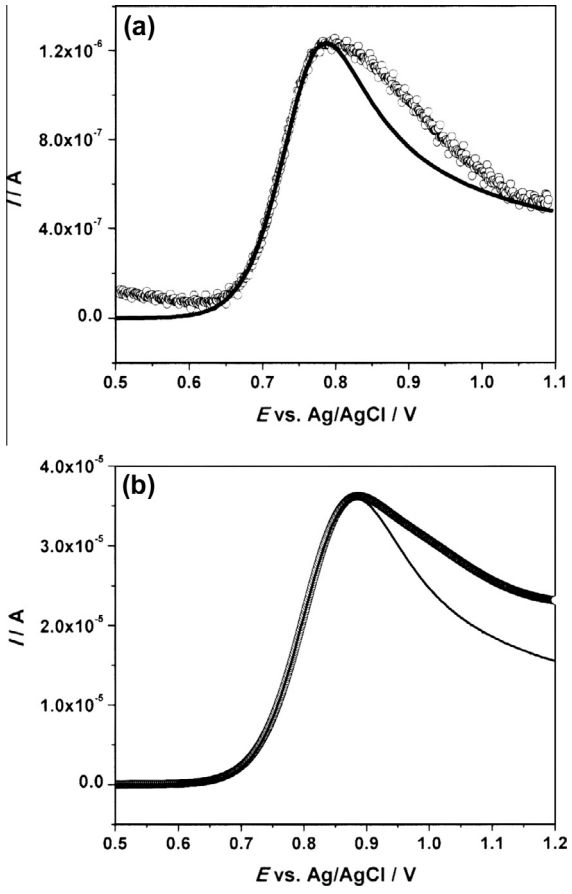

Fig. 7. Theoretical simulated (solid line) and experimental (*o*) linear sweep voltammograms obtained by the fitting procedure (see text). c^*_{MON}: (a) 1×10^{-4} - mol dm^{-3}; (b) 3×10^{-3} mol dm^{-3}. $\upsilon = 0.100$ V s^{-1}. Working electrode: EPGCE.

the difficulties in performing a good correction of blank current on voltammograms obtained on EPGCE, mainly for solutions of low reactant concentration, which makes the process of fitting the experimental and simulated voltammograms a rather complicated task.

The comparison between Ψ_T and Ψ_E with $\upsilon^{1/2}$ for the mechanism indicated previously is shown in Fig. 4. The range of scan rates was from 0.025 to 0.4 V s^{-1}. The three solutions of highest concentrations were used to confirm the proposed mechanism. Ψ_E values of a solution of low concentration, i.e. 4.2×10^{-5} - mol dm^{-3}, are also included to show the greatest effect of adsorption at lower concentrations of MON where higher currents are obtained, i.e., Ψ_E are higher than those corresponding to solutions of higher concentrations. Simulated values agree quite well with experimental results.

The parameters of the different steps of the reaction mechanism, such as heterogeneous formal rate constant (k_f^o) and formal potential (E_f^o) for the electrochemical reaction (Eq. (5) in Scheme 1), rate and equilibrium constants of chemical steps (Eqs. (4 and 6) in Scheme 1) were calculated from the best fitting of experimental and simulated cyclic voltammograms. To start the fitting procedure through BAS DigiSim® software, anodic transfer coefficient (α) for the heterogeneous electron transfer reaction was assumed constant and equal to 0.5. D_{MON} was also kept constant and equal to 4.8×10^{-6} cm^2 s^{-1} (see above). Diffusion coefficients of all other species were also kept constant at the same value as MON, except for D_{H^+}, which was assumed to be $D_{H^+} = 1 \times 10^{-5}$ cm^2 s^{-1} [26]. After a first trial where the value of k_f^o converges to $(1.3 \pm 0.7) \times 10^{-2}$ cm s^{-1}, it was kept constant for the following fitting procedures to calculate the other parameters. The thermodynamic and kinetics parameters obtained from the best fitting were: $E_f^o = (0.815 \pm 0.003)$ V, $k_f^o = (1.3 \pm 0.7) \times 10^{-2}$ cm s^{-1}, $K(1) = 10^{-3}$ mol dm^{-3}, $k_f(1) = (7 \pm 0.3) \times 10^4$ s^{-1}, $K(2) = 10^5$ - mol dm^{-3}and $k_f(2) = (1.6 \pm 0.1) \times 10^2$ s^{-1}, where (1) and (2) refers to homogeneous chemical reactions indicated by Eqs. (4 and 6) in Scheme 1. The formal rate constant for the heterogeneous electron transfer step conforms well to the quasi-reversible redox couple as expected for the electrooxidation of carbonyl compounds, when the constituents of the redox couple are similar in structure and size in polar non-aqueous solvents [27]. The value for the apparent acid constant of MON in ACN medium, $K(1) \leqslant 10^{-3}$ (Eq. (4) in Scheme 1) obtained from fitting is reasonable, as compared with the one reported in literature for MON in aqueous medium, where it behaves as a rather strong acid, i.e. $pK_a \approx 0$ [1]. It is well known that acidic properties of substrates are diminished in non-aqueous solvents of lower basicity than those in water [27]. On the other hand, the value found for $k_f(2)$ agrees very well with the appearance of the cathodic peak at the sweep rates indicated above, corresponding to a chemical kinetics step not so fast.

The radical generated by the electrochemical oxidation of MON^- in ACN would be a species stabilized by resonance, i.e., structures a–c in Scheme 2:

This phenomenon might explain the fact that, at relatively low sweep rates ($\upsilon \sim 50$ V s^{-1}), the complementary cathodic peak of the MON redox system starts to appears after the potential scan

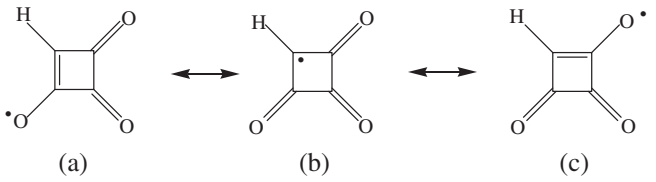

Scheme 2.

is reversed in the voltammetric experiment. On the other hand, UV–vis spectra recorded immediately after the exhaustive electrolysis of MON at controlled potential showed the disappearance of both absorption bands characteristic of the mycotoxin, i.e., $\lambda_{1,max}$ = 229 nm ($\varepsilon = 2.27 \times 10^4$ mol^{-1} dm^{-3} cm^{-1}) and $\lambda_{2,max}$ = 276 nm ($\varepsilon = 5.38 \times 10^3$ mol^{-1} dm^{-3} cm^{-1}). This behavior would indicate that the chromophore group of the parent molecule, i.e., the carbonyl α–β unsaturated group is lost in the MON electrochemical oxidation. Therefore, we consider probable that species P and Z in Scheme 1 would be acetic acid and CO_2, respectively, according to the proposal of Franck and Breipohl for the decomposition of MON in 2% H_2O_2 solutions [28].

3.2. Controlled potential electrolysis

Controlled potential electrolysis was carried out at 1.10 V during 1.8×10^3 s. Amperometric responses recorded for the blank solution and a MON solution at $c^*_{MON} = 8.3 \times 10^{-5}$ mol dm^{-3} during and after performing the electrolysis are shown in Fig. 8a. The current–time transient recorded after electrolysis for MON solution is almost the same as that recorded for the blank solution, putting in evidence the total mycotoxin consumption during the experiment. In addition, this behavior can also be inferred from cyclic voltammograms recorded before and after electrolysis (compare curves 1 and 2 in Fig. 8b. A value of n = 1.1 was determined as the number of electrons exchanged per mole of electrolyzed substance from the charge (Q) measured.

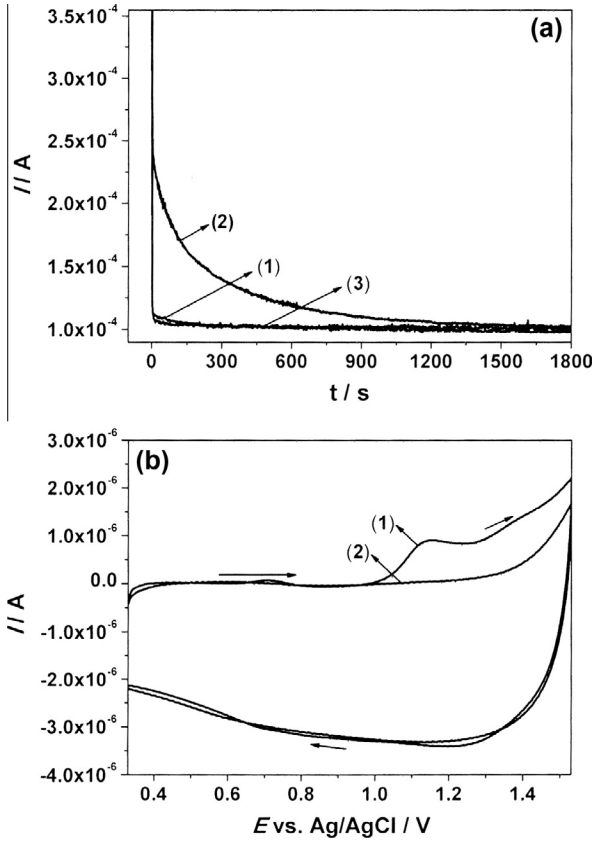

Fig. 8. (a) Amperometric responses obtained at: (1) the blank solution (ACN + 0.1 mol dm^{-3} $(H_9C_4)_4NF_6P$), (2) and (3) a MON solution during and after electrolysis, respectively. (b) Cyclic voltammograms of MON recorded before (1) and after (2) performing the controlled potential electrolysis. $c^*_{MON} = 8.3 \times 10^{-5}$ mol dm^{-3}. v = 0.050 V s^{-1}. Working electrode: EPGCE. Arrows indicate the direction of sweep potential.

3.3. Determination of MON in pure solvent

Calibration curves of adsorbed MON SWV responses at very low substrate bulk concentrations are discussed here for its analytical applications to perform the MON determination in real infected matrixes. The net current ($I_{p,n}$)-potential curve in SWV is the most useful analytical signal [29,30]. The high sensitivity of adsorptive accumulation methods is obviously its greatest advantage. Besides, the adsorptive accumulation is analytically useful only if the portion of the electrode surface covered by the adsorbed reactant is small (about 20% of the total area). Under this condition, the relationship between the surface concentration of the adsorbed analyte and its bulk concentration may be considered as approximately linear [30]. The combination of adsorptive accumulation with SWV provides to be an electroanalytical tool very valuable for performing trace analysis of compounds, which are both surface active and electroactive.

The determination of MON was carried out at an EPGCE in unstirred ACN + 0.1 mol dm^{-3} $(H_9C_4)_4NPF_6$ solutions after an accumulation time (t_{acc}) of 300 s by using an accumulation potential, E_{acc} = 0.7 V. Typical SW voltammograms are shown in Fig. 9. A linear relationship between $I_{p,n}$ vs. c^*_{MON} was obtained at f = 10 Hz in the range from 1.1×10^{-11} mol dm^{-3} to 1.6×10^{-9} mol dm^{-3}. The linear regression can be expressed by a least square procedure as:

$$I_{p,n} = (2.43 \pm 0.22) \times 10^3 c^*_{MON} + (7.8 \pm 0.9) \times 10^{-7} \quad (r = 0.9835) \tag{8}$$

In Eq. (8), $I_{p,n}$ is expressed in amperes and c^*_{MON} in moles dm^{-3}. Data used in the regression analysis of the calibration curve are the average of three replicated measurements (six experimental points were taken into account). The detection limit (dl) measured experimentally for a signal to noise ratio of 3:1 was 1×10^{-11} mol dm^{-3} (1.2 ng dm^{-3}).

No data comparison on both electrochemical and electroanalytical properties of MON with other in the literature is possible, given that data shown in this work are the first to our knowledge in this regard. In principle, the value of detection limit for MON reported in this article compares favorably well with respect to those of chromatographic techniques previously reported. Indeed, it is significantly lower than those informed in literature, i.e. 0.12 μg dm^{-3} [31], 0.7 μg dm^{-3} [13] and 1 μg dm^{-3} [11,32] among others [12]. The significant difference in detection limits shows clearly that adsorption (pre-concentration) of MON on EPGCE in non-aqueous media from very low concentration solutions and its electrochemical discharge is a very efficient process. Results obtained in this

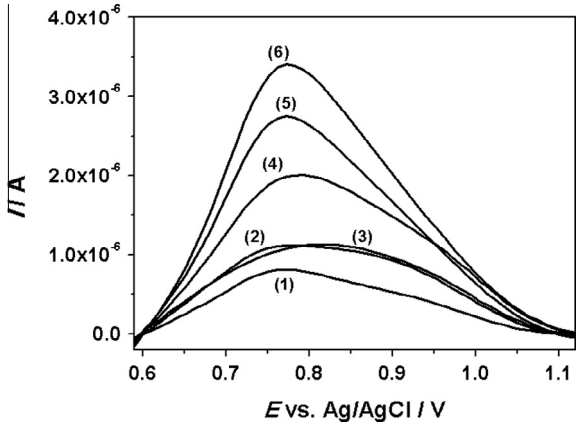

Fig. 9. Square wave voltammograms of MON in ACN + 0.1 mol dm^{-3} $(H_9C_4)_4NPF_6$ at EPGCE. c^*_{MON}: (1) 1.05×10^{-11}; (2) 7.87×10^{-11}; (3) 1.95×10^{-10}; (4) 5.4×10^{-10}; (5) 7.66×10^{-10}; (6) 1.43×10^{-9} mol dm^{-3}.

work clearly establish a challenge to develop a new methodology for the determination of MON in real samples based on adsorptive SWV.

4. Conclusions

The electrochemical oxidation of moniliformin mycotoxin is studied for the first time. A complex electro-oxidation mechanism can be inferred from results obtained by cyclic and square wave voltammetries from measurements carried out in a non-aqueous reaction medium, where both the weak adsorption of the mycotoxin at the electrode surface and the presence of chemical reactions coupled to the initial charge transfer reaction are present.

Based on experimental results, and those obtained by digital simulation, we propose a probable mechanism for the electrochemical oxidation of moniliformin. Therefore, thermodynamic and kinetics parameters were calculated from digital simulation of cyclic voltammograms.

On the other hand, square wave voltammetry was used to perform the mycotoxin quantitative determination where a very low detection limit was found, showing to be an important analytical tool as an alternative to other techniques commonly used to determine moniliformin in real matrices.

Conflict of interest

The authors declare that there is no conflict of interest.

References

[1] J.M. Soriano del Castillo, Micotoxinas en alimentos, Ediciones Díaz de Santos, España, 2007.
[2] R.J. Cole, J.W. Kirksey, H.G. Cutler, B.L. Doupnik, J.C. Peckham, Science 179 (1973) 1324–1326.
[3] J.P. Springer, J. Clardy, R.J. Cole, R.W. Kirksey, R.K. Hill, R.M. Carlson, J.L. Isidor, J. Am. Chem. Soc. 96 (1974) 2267–2268.
[4] M. Steyn, P.G. Thiel, G.C. Van Shalkwyk, J. AOAC Int. 61 (1978) 578–580.
[5] M. Jonsson, M. Jestoi, A.V. Nathanail, U.-M. Kokkonen, M. Anttila, P. Koivisto, P. Karhunen, K. Peltonen, Food Chem. Toxicol. 53 (2013) 27–32.
[6] N.P. Kriek, W.F. Marasas, P.S. Steyn, S.J. van Rensburg, M. Steyn, Food Cosmet. Toxicol. 15 (1977) 579–587.
[7] P.G. Thiel, Biochem. Pharmacol. 27 (1978) 483–486.
[8] L.T. Burka, J. Doran, B.J. Wilson, Biochem. Pharmacol. 31 (1982) 79–84.
[9] M.C. Pirrung, S.K. Nauhaus, J. Org. Chem. 61 (1996) 2592–2593.
[10] M. Jestoi, Crit. Rev. Food Sci. Nutr. 48 (2008) 21–49.
[11] V. Scarpino, M. Blandino, M. Negre, A. Reyneri, F. Vanara, Food Addit. Contam. 30 (2013) 876–884.
[12] R. Krska, E. Welzig, H. Boudra, Anim. Feed Sci. Technol. 137 (2007) 241–264.
[13] K.W. von Bargen, L. Lohrey, B. Cramer, H. Humpf, J. Agric. Food Chem. 60 (2012) 3586–3591.
[14] G.J.C. Vidal, L. Bonel, A. Ezquerra, S. Hernández, J.R. Bertolín, C. Cubel, J.R. Castillo, Biosens. Bioelectron. 49 (2013) 146–158.
[15] M.A. Zon, N.C. Marchiando, H. Fernández, J. Electroanal. Chem. 465 (1999) 225–233.
[16] R.H. Wopschall, I. Shain, Anal. Chem. 39 (1967) 1514–1527.
[17] R.S. Nicholson, I. Shain, Anal. Chem. 36 (1964) 706–723.
[18] A.J. Bard, L.R. Faulkner, Electrochemical Methods. Fundamentals and Applications, second ed., John Wiley & Sons, USA, 2001.
[19] B.E. Conway, D.C.W. Kannangara, J. Electrochem. Soc. 134 (1987) 906–918.
[20] J.C. Imbeaux, J.M. Saveant, J. Electroanal. Chem. 44 (1973) 169–187.
[21] R.H. Wopschall, I. Shain, Anal. Chem. 39 (1967) 1535–1542.
[22] C.P. Andrieux, L. Nadjo, J.M. Saveant, J. Electroanal. Chem. 26 (1970) 147–186.
[23] C.P. Andrieux, L. Nadjo, J.M. Saveant, J. Electroanl. Chem. 42 (1973) 223–242.
[24] L. Nadjo, J.M. Saveant, J. Electroanl. Chem. 44 (1973) 327–366.
[25] V.D. Parker, Acta Chem. Scand. 52 (1998) 154–159.
[26] R. Sereno, Ph D Thesis, Universidad Nacional de Córdoba, Argentina, 1972.
[27] K. Izutsu, Electrochemistry in Non Aqueous Solutions, Wiley-VCH, New York, USA, 2002.
[28] B. Franck, G. Breipohl, Angew. Chem. Int. Ed. Engl. 23 (1984) 996–998.
[29] N.C. Marchiando, M.A. Zon, H. Fernández, Anal. Chim. Acta 550 (2005) 199–203.
[30] V. Mirceski, S. Komorsky-Lovric, M. Lovric, Square wave voltammetry. Theory and application, in: F. Scholz (Ed.), Monographs in Electrochemistry, Springer, Leipzig, Germany, 2007.
[31] W. Kandler, M. Nadubinska, A. Parich, R. Krska, Anal. Bioanal. Chem. 374 (2002) 1086–1090.
[32] J.L. Sørensen, K.F. Nielsen, U. Thrane, J. Agric. Food Chem. 55 (2007) 9764–9768.